ChemCatChem

Research Article
doi.org/10.1002/cctc.202200627

Chemistry Europe
European Chemical Societies Publishing

www.chemcatchem.org

Influence of Framework *n*(Si)/*n*(Al) Ratio on the Nature of Cu Species in Cu-ZSM-5 for NH_3-SCR-DeNO$_x$

Magdalena Jabłońska,*[a] Kinga Góra-Marek,[b] Paolo Cleto Bruzzese,[c] Ana Palčić,[d] Kamila Pyra,[b] Karolina Tarach,[b] Marko Bertmer,[c] David Poppitz,[a] Andreas Pöppl,[c] and Roger Gläser[a]

Nanosized Cu-containing ZSM-5 catalysts with different *n*(Si)/*n*(Al) ratio of 18.9–50.5 were prepared by ion-exchange. The physico-chemical characterization clearly shows that the molar ratio of framework T atoms influences the nature and distribution of copper species. According to DR UV-Vis, TPR-H_2, EPR, or FT-IR spectroscopy analyses, the amount of aggregated copper species increases with increasing the framework *n*(Si)/*n*(Al) ratio. Thus, the activity of the Cu-containing ZSM-5 with *n*(Si)/*n*(Al) ratio of 47.0—50.5 in the selective catalytic NO reduction with NH_3 (NH_3-SCR-DeNO$_x$) significantly decreases compared to the other materials (*n*(Si)/*n*(Al) ratio of 18.9—19.6). The reaction mechanism has been discussed in light of the results of 2D COS (two-dimensional correlation spectroscopy) analysis of IR spectra and catalytic properties of the zeolites. The results make evident that enhanced activity of Cu-containing ZSM-5 in NH_3-SCR-DeNO$_x$ is correlated with the formation of different NO_x^- under the experimental conditions.

Introduction

Nitrogen oxides (NO, NO_2 and N_2O) originating from combustion processes are typical air pollutants, which cause various human health issues and way negatively impact the environment. Among the NO_x emission control technologies, the selective catalytic reduction of NO with NH_3 (NH_3-SCR-DeNO$_x$) is the most common method to catalytically reduce NO_x in flue gases from stationary as well as mobile sources. NO_x present in the flue gases are selectively reduced by NH_3 to N_2 and H_2O, i.e., the desired products of this process. The V_2O_5-WO_3/TiO_2 metal oxide system serves as the major industrial catalyst for NH_3-SCR-DeNO$_x$ that effectively operates in a relatively narrow temperature range from 300 to 400 °C.[1–3] Otherwise, copper-based small pore molecular sieves with chabazite (CHA) framework, such as Cu-SAPO-34 and Cu-SSZ-13 have received wide attention in systems for the removal of NO_x and have been commercialized as the NH_3-SCR-DeNO$_x$ catalysts in diesel engines due to their superior activity, improved hydrothermal stability, and alkali metal resistance.[4–6] The copper-containing zeolite-based catalysts operate in low-temperature NH_3-SCR-DeNO$_x$ (below 400 °C), however, the controlled deposition of copper species is necessary. The *n*(Si)/*n*(Al) ratio is one of the main factors extensively investigated over Cu-CHA. For instance, Gao et al.[7] found that the Cu^{2+} location in SSZ-13 and the concentration of the Brønsted acid sites are closely related to the *n*(Si)/*n*(Al) ratio (among 6, 12, and 35). In the following studies, Cu-containing SSZ-13 with *n*(Si)/*n*(Al) within a range of 13–15 (compared with the materials having *n*(Si)/*n*(Al) = 6–30) prepared by the one-pot method were reported as the most active, selective and stable catalysts in NH_3-SCR-DeNO$_x$.[8,9] The physico-chemical characterization of these catalysts confirmed that the *n*(Si)/*n*(Al) ratio influences the nature and the distribution of copper species but also affects the concentration of acid sites of the catalysts. Furthermore, Feng et al.[8] claimed that the number and the intensities of the adsorbed species, i.e., NH_3 adsorption states and the NO_x^- species, on the catalyst surface on Cu-SSZ-13 were closely related to the *n*(Si)/*n*(Al) ratio on the grounds of DRIFTS spectroscopy results. As stated above, the effect of *n*(Si)/*n*(Al) over Cu-CHA catalysts in NH_3-SCR-DeNO$_x$ is broadly investigated compared to the other zeolite topologies, including MFI[10] or BEA.[11] E.g., Torre-Abreu et al.[10] studied commercial Cu-ZSM-5 with *n*(Si)/*n*(Al) of 11–100 as the catalysts for the selective catalytic reduction of NO_x by propene (C_3H_6-SCR). They found that for the materials with a lower ratio of framework T atoms, *n*(Si)/*n*(Al), the copper species exist mainly in the form of isolated Cu^{2+} (main active sites for C_3H_6-SCR), while the increase in the ratio led to the formation of isolated Cu^+/Cu^{2+} together with CuO aggregates.

The most recently available literature focuses on the investigation of the reaction mechanism over Cu-CHA or Cu-

[a] Dr. M. Jabłońska, Dr. D. Poppitz, Prof. Dr. R. Gläser
Institute of Chemical Technology
Universität Leipzig
Linnéstr. 3, 04103 Leipzig (Germany)
E-mail: magdalena.jablonska@uni-leipzig.de
[b] Prof. Dr. K. Góra-Marek, Dr. K. Pyra, Dr. K. Tarach
Faculty of Chemistry
Jagiellonian University in Krakow
Gronostajowa 2, 30-387 Krakow (Poland)
[c] P. C. Bruzzese, Dr. M. Bertmer, Prof. Dr. A. Pöppl
Felix Bloch Institute for Solid State Physics
Universität Leipzig
Linnéstr. 5, 04103 Leipzig (Germany)
[d] Dr. A. Palčić
Laboratory for the Synthesis of New Materials,
Division of Materials Chemistry, Ruđer Bošković Institute
Bijenička 54, 10000 Zagreb (Croatia)

Supporting information for this article is available on the WWW under https://doi.org/10.1002/cctc.202200627

based oxides in NH_3-SCR-DeNO$_x$.[12–14] Generally, NH_3-SCR-DeNO$_x$ is based on the Cu^+/Cu^{2+} redox cycle, where Cu^{2+} is reduced by NH_3 and/or NO and Cu^+ is oxidized by O_2 (which is considered as the rate-determining step). Cu^+/Cu^{2+} species are solvated by two NH_3-ligands forming mobile $Cu(NH_3)^{2+}$, $Cu(NH_3)_4^{2+}$, $Cu(OH)(NH_3)^{3+}$ complexes, and complexes containing a mixture of NH_3 and NO_x ligands, e.g., $[Cu(OH)(NH_3)_3(NO)]^+$ – for the first time spectroscopically approved over Cu-containing zeolite-based catalysts by Tarach et al.[12] According to the widely accepted NH_3-SCR pathways (e.g.,[12,15]), upon the formation of $[Cu(OH)(NH_3)_3(NO)]^+$ intermediates, the neighboring NH_3 and NO ligands will rearrange to create N–N bond *via* the nitrosamine (NH_2NO) or ammonium nitrite (NH_4NO_2) intermediates. NH_2NO and NH_4NO_2 will subsequently decompose into N_2 and H_2O to complete the reduction part of NH_3-SCR-DeNO$_x$.[13] The mechanism of NH_3-SCR-DeNO$_x$ has been explored mainly by the application of *in situ* FT-IR spectroscopy. Infrared spectroscopy is a valuable method of tracking the reaction mechanism of reagents whose chemisorbed states can be identified in the spectrum as specific diagnostic bands. In 2D correlation spectra, in contrast to 1D conventional spectra, the overlapping peaks are significantly better resolved and only the IR characteristics of the mutual dependent species are revealed which finally allows their easier detecting and concluding on the specific sequential order of spectral intensity changes.

Our earlier study[12] shows that the Cu-ZSM-5 catalyst (among Cu-TNU-9, Cu-FER, Cu-Y) displays an extraordinary activity in NH_3-SCR-DeNO$_x$ achieving the 100% conversion at 175 °C with almost 100% selectivity for the formation of N_2. The framework geometry (MFI, TUN, FER, FAU) was found as a factor in deciding on the copper sites accessibility and the saturation with ammonia molecules while the *n*(Si)/*n*(Al) ratio (2.5–15) governs the copper sites speciation and ammonium ions stabilization. Otherwise, the effect of molar ratio on NO_x^- formation was less extensively investigated to gain insight into the possibility of nitrate formation not dependent on the type of the structure itself, but the number of Al atoms (thus, the content of Cu^{2+} species).

Thus, in this work, the Cu-containing nanosized ZSM-5 with different *n*(Si)/*n*(Al) ratio of 18.9–50.5 are prepared and tested for their activity and selectivity in NH_3-SCR-DeNO$_x$. In general, the incorporation of T atoms (e.g., Si, Al, P, B, Ge, etc.) in zeolite framework in terms of occupation of specific crystallographic position (T sites), a certain region of the crystal as well as their quantity, i.e., *n*(Si)/*n*(T) ratio, is determined by the nature of the T atom itself, the source chemicals of the each T atom, the chemical composition of the reaction mixture (e.g., initial *n*(Si)/*n*(T) ratio, pH), the type of mineralizer as well as the reaction conditions (e.g., temperature, agitation, supersaturation, etc.).[16–19] Herein, the variations in the framework *n*(Si)/*n*(Al) ratio were achieved *via* changes in the zeolite preparation temperature. The Cu-containing zeolites were characterized in terms of their structure and morphology (XRD, SEM, TEM, ICP-OES, NMR), texture (N_2 sorption), acidity (FT-IR studies of pyridine (Py) sorption), the nature of the copper species (DR UV-Vis, TEM and EPR) and were investigated as the catalysts for the NH_3-SCR-DeNO$_x$. In order to determine the effect of the *n*(Si)/*n*(Al) ratio on the catalytic activity and thus, to well define the mechanism of NH_3-SCR-DeNO$_x$ on Cu-containing catalysts at low temperature, we applied 2D COS (two-dimensional correlation spectroscopy) analysis of time-resolved IR spectroscopy that enables following even the slightest changes in the spectra of reagents adsorbed over studied zeolites.

Results and Discussion

Structural, textural and acidic properties

Figure 1 presents the powder XRD patterns of the investigated Cu-containing ZSM-5 series of the samples. The diffraction patterns of synthesized solids exhibit the diffraction peaks characteristic of MFI-type materials. Furthermore, the SEM images (Figure 2) of the studied Cu-containing ZSM-5 samples prove the typical morphology of MFI-type zeolite materials. The presence of large aggregates out of homogeneously ball-shaped particles was observed. The average particle size in each sample was determined as the average of 300 measured particles in the SEM images. It was found that the size of the ZSM-5 particles ranges from 50 to 300 nm. In contrast, the commercially-based material exhibits particles showing a much broader particle size distribution ranging from 50 to 800 nm. These findings are corroborated by TEM analysis exemplary shown for sample Cu-ZSM-5-170. The analyzed crystals have a typical coffin shape and the size of the crystals corresponds to the size determined from SEM data. High-resolution TEM gives lattice plane imaging representing the evidence of high crystallinity of the particles. In addition, TEM-EDX experiments show the presence of copper species in all investigated positions. Average mass fractions of 3.8 wt.% and 5.3 wt.% were determined for Cu-ZSM-5-100 and Cu-ZSM-5-170, respectively. Imaging of copper species in TEM (Figure 2d, SI1a) or in scanning-TEM (STEM) material contrast imaging (Figure SI1b) evidenced the presence of copper species with 0.5–3 nm size dispersed evenly throughout the zeolite crystal. This leads to

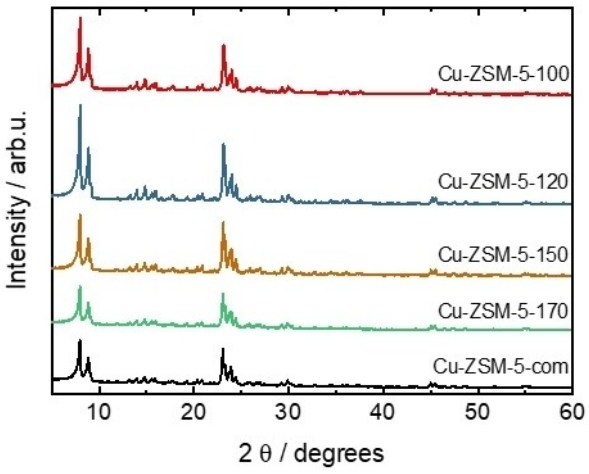

Figure 1. XRD patterns of Cu-containing ZSM-5 (sample labels as in Table 1).

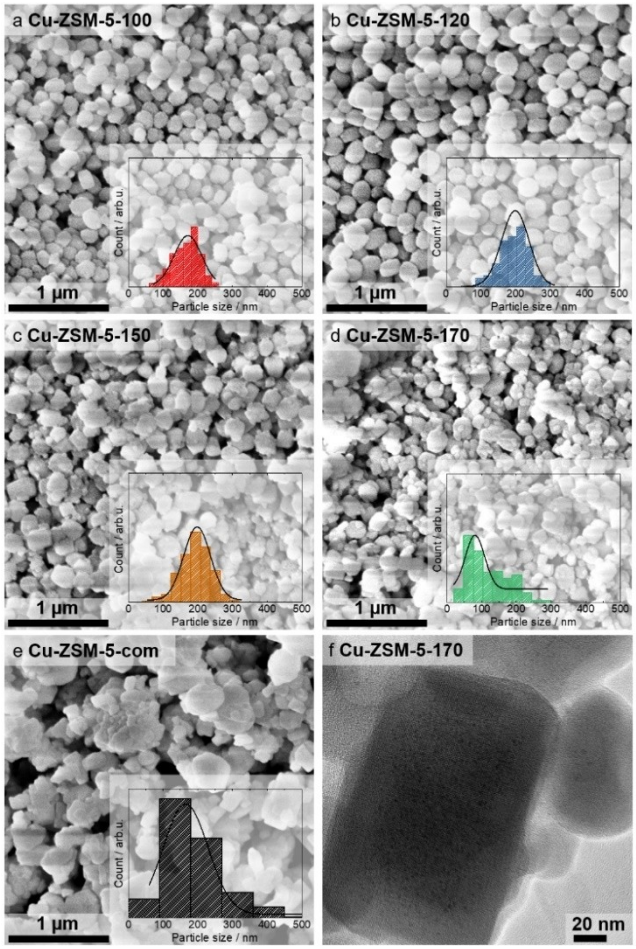

Figure 2. SEM images of Cu-containing ZSM-5 (a–e) and TEM (f) image of Cu-ZSM-5-170. The zeolite particle size distribution (inlay in a–e) was obtained by counting 300 particles from SEM images.

the assumption that copper oxo-species are homogeneously distributed within the crystallites. Such high dispersion of oxo-species allows concluding on the presence of even more finely dispersed copper species of the size below the detection limit of the TEM (atomic distribution), including the exchangeable Cu^{+} and Cu^{2+} cations.

The copper content in the samples, considering that the same ion-exchange procedure was applied, differs depending on the zeolite synthesis temperature. For ZSM-5 synthesized at 100 and 120 °C, the ICP-OES analysis (Table 1) reveals 3.2–3.5 wt.% of Cu. A lower amount of copper species (2.5–2.7 wt.% of Cu) is found for the materials treated at higher temperatures (i.e., 150–170 °C) as well as for commercial ZSM-5 (2.1 wt.% of Cu). The n(Cu)/n(Al) ratio determined by ICP-OES analysis varies among materials from 0.5 to 2.1, which shows that the ZSM-5 synthesized at lower temperatures enabled the introduction of a greater amount of copper species with the same method used. Further, in all cases, there is more Cu than Al species which means that more Cu species are present than expected according to the Al species quantity (n(Cu)/n(Al) is $\geq$ 0.5). Namely, one should keep in mind that Al in the zeolite framework bears the negative charge which requires charge-compensating cation. Thus, in the case of n(Cu)/n(Al) = 0.5 the total negative zeolite framework charge would be compensated. It indicates that conducting the ion-exchange at room temperature (RT, ca. 25 °C) causes a strong binding of $[Cu(OH)(H_2O)_n]^{+}$ species formed by hydrolysis prior to/during the ion-exchange process at the external surface of the zeolites. These surface species are transformed by calcination into oxides characterized by low acid strength (see FT-IR studies of Py sorption). Although the materials Cu-ZSM-5-100 and Cu-ZSM-5-120 have a lower total aluminum content, still there is higher amount of copper species introduced than in Cu-ZSM-5-150(170). This effect is attributed to the greater specific surface area of the materials prepared at lower temperature that provides more potential binding sites and respective higher number of the defect sites that afford suitable environment for strong interactions with various Cu species present in the ion-exchange solution.

Figure 3 presents the N_2-sorption isotherms and pore width distribution of Cu-containing ZSM-5. The nanosized materials display mixed type I and type IV isotherms with a very steep and almost parallel hysteresis (H1 type) in the range of p p_0^{-1} > 0.8. The specific surface area values vary in the range of 346–374 $m^2 g^{-1}$ (Table 2). Further, there is a significant contribution of mesopores to the total pore volume of the studied samples. BJH analysis revealed that the size of mesopores for the materials with ZSM-5 prepared at the lower temperatures lies in the range of 20–50 nm, while in the case of the materials prepared at 150 and 170 °C the range is 35–60 nm. By means of TEM imaging, only the presence of microporosity could be found within the ZSM-5 crystals. This leads to the assumption, that these relatively large pores measured by BJH analysis arise from interparticle porosity.

Solid-state NMR spectra of the studied series of the samples are shown in Figure 4. According to the ^{27}Al MAS NMR spectra, all of the aluminum is embedded in the zeolite framework as evidenced by the resonances arising at 54 ppm for tetrahedrally coordinated aluminum in agreement with previous studies.[20–22] Other studies have further analyzed the presence of different T

Table 1. Results of elemental analysis of the studied Cu-containing ZSM-5 by ICP-OES: (ω_i mass fractions).

Samples	ω_{Si}/wt.%	ω_{Al}/wt.%	ω_{Cu}/wt.%	n(Si)/n(Al)	n(Cu)/n(Al)
Cu-ZSM-5-100	39.1	0.8	3.2	47.0	1.7
Cu-ZSM-5-120	36.8	0.7	3.5	50.5	2.1
Cu-ZSM-5-150	43.2	2.2	2.7	18.9	0.5
Cu-ZSM-5-170	36.7	1.8	2.5	19.6	0.6
Cu-ZSM-5-com	40.1	1.3	2.1	29.6	0.7

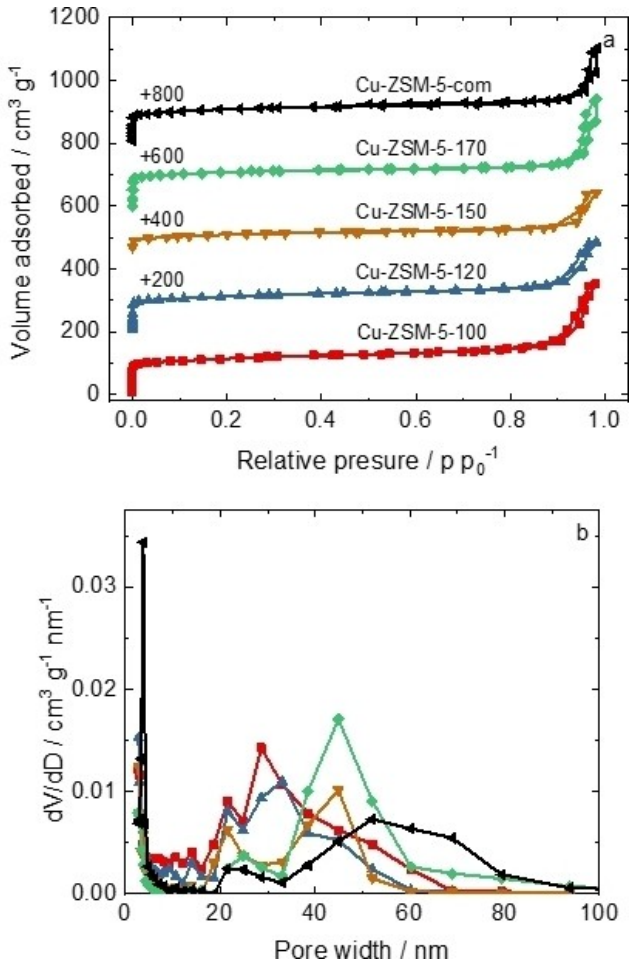

Figure 3. a) N_2-sorption isotherms and b) pore width distribution of Cu-containing ZSM-5.

sites that become visible in 3QMAS studies with the standard MAS spectrum showing only one signal.[23] A shoulder at 60 ppm is observed in the sample where ZSM-5 was prepared at 150 °C representing an indication of the second type of tetrahedral aluminum that accounts for about 6% of the signal. This was assigned to different T-sites of the zeolite lattice.[24] In general, also the linewidth increases with reaction temperature which could also hint at diversification of aluminum sites.

Signals in the range from −110 ppm to −119 ppm in ^{29}Si MAS NMR spectra of the nanosized samples pinpoint that in these materials the silicon is dominantly surrounded by four Si atoms bonded *via* shared oxygen atoms (Q^4, Si-[$(OSi)_4$]) in agreement with previous studies.[7–9] Another resonance ranging from −100 ppm to −109 ppm could arise due to Q^3 silicon species ((HO)-Si-[$(OSi)_3$]) as well as due to Si with one Al as the adjacent T atom ([$(OSi)_3$]-Si-[OAl]).

The observed profiles are a result of overlapping signals of these moieties. It should be noted that the maximum of this band in the samples with ZSM-5 prepared at 100 °C and 120 °C, is shifted upfield (−103 ppm) whereas the commercial sample and the samples prepared at 150 °C and 170 °C present a maximum at −107 ppm. Taking into consideration the higher Al content in the samples prepared at higher temperatures and previous findings (e.g.,[25]), it can be concluded that in the samples prepared at lower temperatures the Q^3 species account for the dominant contribution to the −100 to −109 ppm signal. This represents an indication that more silanol defects are formed in the materials prepared at lower temperatures as confirmed by ^{1}H→^{29}Si CP NMR spectra where the peak maximum arises at −102−−103 ppm (Figure SI2). This statement can be further supported by the linear dependence of the intensity of the Si-OH group band on the corresponding specific surface area ($A_{S(BET)}$, Table 2, Figure 4c). Indeed, in the materials synthesized at lower temperatures the external surface area is more populated with isolated silanol defects (Figure SI3).

Acidic properties of Cu-containing ZSM-5 were assessed in quantitative IR studies of pyridine sorption (Table 3). This strongly basic molecule is widely used to determine the nature and the concentration of the Brønsted and Lewis acidic sites

Table 2. Textural properties determined from the N_2-sorption isotherms: specific surface area ($A_{S(BET)}$), specific total pore volume ($V_{(TOT)}$), micropore ($V_{(MIC)}$), and mesopore volume ($V_{(MES)}$).

Samples	$A_{S(BET)}$/m² g⁻¹	V_{MIC}/cm³ g⁻¹	V_{MES}/cm³ g⁻¹	V_{TOT}/cm³ g⁻¹
Cu-ZSM-5-100	374	0.14	0.40	0.54
Cu-ZSM-5-120	367	0.15	0.29	0.44
Cu-ZSM-5-150	352	0.15	0.23	0.38
Cu-ZSM-5-170	346	0.15	0.38	0.53
Cu-ZSM-5-com	354	0.14	0.33	0.47

Table 3. Acidic properties of the samples determined from pyridine sorption: concentration of Brønsted and Lewis sites, respectively ($C_{Brønsted}$, C_{Lewis}), total concentration (C_{Total}), and the acid strength of sites (py_{170}/py_{130}).

Samples	$C_{Brønsted}$/μmol g⁻¹	C_{Lewis}/μmol g⁻¹	C_{Total}/μmol g⁻¹	py_{170}/py_{130}	
	130/170 °C	130/170 °C	130/170 °C	$C_{Brønsted}$	C_{Lewis}
Cu-ZSM-5-100	0/0	849/453	849/453	–	0.53
Cu-ZSM-5-120	0/0	786/528	786/528	–	0.64
Cu-ZSM-5-150	91/85	1158/650	1249/735	0.93	0.82
Cu-ZSM-5-170	108/102	1318/1151	1426/1253	0.94	0.87
Cu-ZSM-5-com	96/91	1459/1220	1555/1311	0.94	0.84

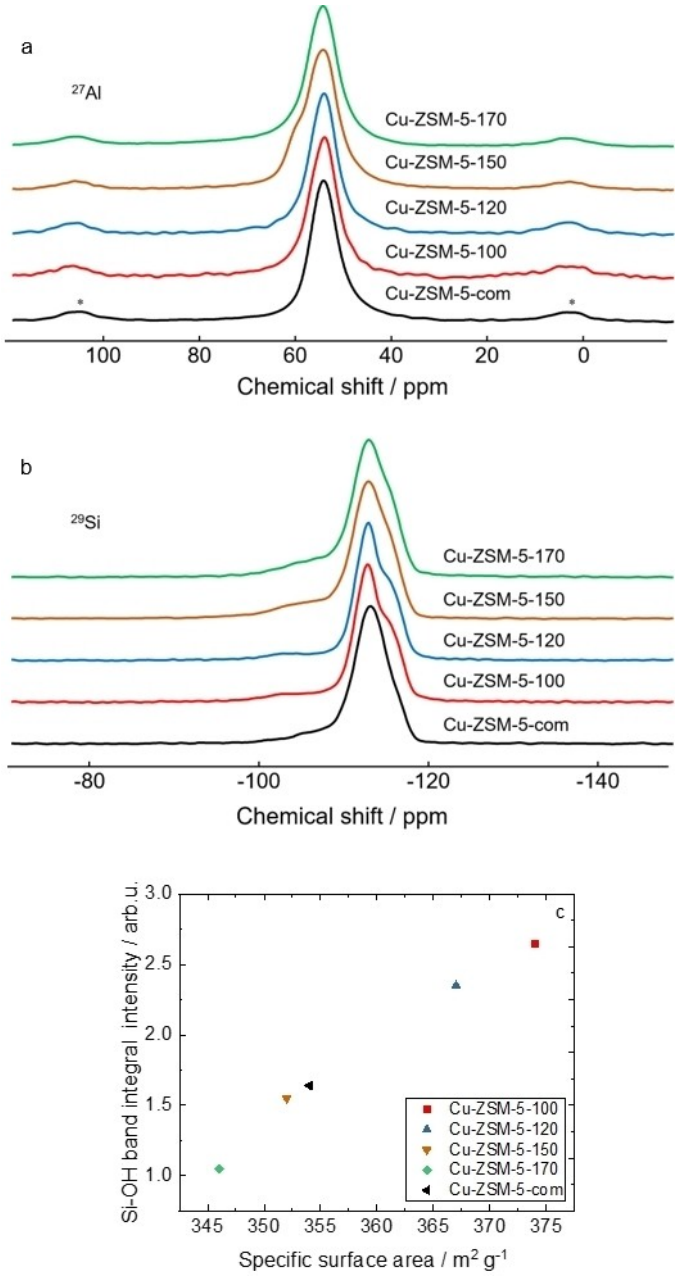

Figure 4. a) ^{27}Al MAS, b) ^{29}Si MAS spectra of Cu-containing ZSM-5; spinning sidebands are indicated for the lowest spectrum only by asterisks, and c) dependence of the intensity of the Si-OH groups' band (3750–3730 cm^{-1}) in the FT-IR spectra on the specific surface area.

populated in the solid catalysts. Interaction of Py with Brønsted sites results in the transfer of proton to Py molecule and the formation of pyridinium ions identified by the bands at 1550–1540 cm^{-1}. On the other hand, the Lewis acid sites as electron-pair acceptor species ligate Py molecule coordinatively and the PyL bands are located in the 1460–1430 cm^{-1} region. The position of the PyL band informs on the strength of Lewis sites: the more there are electron acceptors, the higher the position of the PyL band is.

Figure 5 presents the spectra of Py interacting with surface acid sites of the studied materials at two temperatures: 130 and 170 °C. The protonic sites are detected only in materials with ZSM-5 synthetized at 150 and 170 °C and in reference to commercial derived Cu-ZSM-5-com zeolite. Their amount did not however differentiate between these materials, their strength expressed as py_{170}/py_{130} is also pretty similar under the experimental conditions applied for acidity evaluation. The larger discrepancies are observed for Lewis-type acid sites. The electron-acceptor species were detected in the highest amount in the Cu-ZSM-5-com followed by Cu-ZSM-5-170 and Cu-ZSM-5-150 materials. The contribution of Lewis sites in Cu-ZSM-5-100 and Cu-ZSM-5-120 is ca. 40–50% lower compared to other samples.

All these findings indicate that a lower amount of Al in the zeolite framework (higher n(Si)/n(Al) ratio) does not allow the stabilization of copper as the exchangeable cations and the major amount of copper species takes the form of oxides. It finally leads to the lower dispersion of copper sites as can be concluded from n(Cu)/n(Al) values and TPR-H_2 data. As aforementioned, the position of the PyL band informs on the strength of Lewis sites. The position of PyL band remains unchanged regardless of the catalyst composition (n(Si)/n(Al) and n(Cu)/n(Al)). Nevertheless, the results of pyridine thermodesorption studies, expressed as py_{170}/py_{130} indicate clearly that the Lewis sites in Cu-ZSM-5-100 and Cu-ZSM-5-120 are characterized by significantly lower strength than those located in the Cu-ZSM-5-com, Cu-ZSM-5-170, and Cu-ZSM-5-150 materials. These observations suggest that the copper sites offering the lowest strength are located on the external surface of zeolite crystals thus Py molecules can be easily removed by evacuation at 170 °C. This lowest strength of the centers may be due to poorer dispersion of copper species and formation of oxide forms, as manifested in DR UV-Vis and TPR-H_2 studies for Cu-

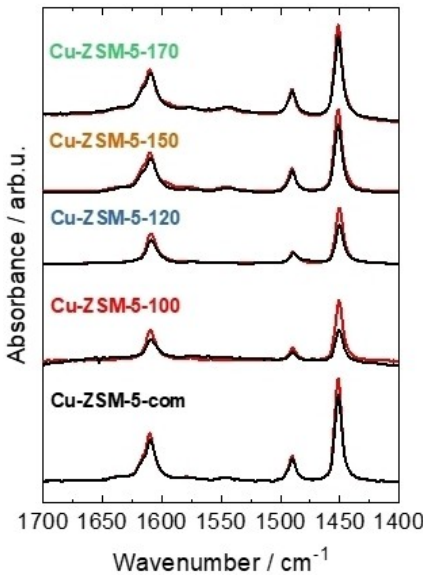

Figure 5. FT-IR spectra of Py interaction with acid sites in Cu-containing ZSM-5 at various temperatures; red line: 130 °C, black line: 170 °C.

ZSM-5-100(120). The consequence is in the binding of reagent molecules, thus NO conversion for these materials will be also lower compared to Cu-ZSM-5-com, Cu-ZSM-5-150(170) materials.

Nature of copper species

The copper ions introduced into ZSM-5 during the ion exchange are initially Cu^{2+} and $Cu(OH)^{+}$ (as a product of hydrolysis of the Cu^{2+} ions in the solution). $Cu(OH)^{+}$ ions are dehydrated at the exchange sites to form isolated Cu^{2+} and $[Cu\text{-}O\text{-}Cu]^{2+}$ species. The *self-reduction* of ion-exchanged Cu^{2+} ions occurs upon thermal activation of the exchanged Cu-ZSM-5 catalyst, as reported earlier (e.g.,[26,27]). The topology and the *n*(Si)/*n*(Al) ratio are the factors influencing the temperature and the rate of Cu^{2+} species reduction, thus speciation of copper in zeolite is differentiated: exciding from isolated Cu^{+} cations to oxide forms of Cu^{+} and Cu^{2+} of various dispersion. As the Cu loading increases, CuO_x species aggregate and grow. Both Cu^{2+} ions and $[Cu\text{-}O\text{-}Cu]^{2+}$ species are considered as the predominant copper species in Cu-ZSM-5 that serve as active species in NH_3-SCR-DeNO$_x$.[12,28] For ZSM-5, Mentzen and Bergeret[29] proposed five exchangeable sites for copper species in the framework. The most populated sites (~60%) are located on the face of the ten-membered ring (MR) (Site II/II′). Site I, Site III, and Site III′ are trapped in secondary five and six ring channel sections of the MFI framework.

The Cu-containing ZSM-5 materials are analyzed concerning the nature and the form of introduced copper species *via* DR UV-Vis, EPR and IR spectroscopy as well as TPR-H_2. Figure 6a shows DR UV-Vis spectra of Cu-containing ZSM-5 (calcined at 550 °C for 4 h in static air). In the case of all samples, distinct peaks are obtained. According to the literature indications, the adsorption bands at about 200–260 nm can be assigned to oxygen-to-metal charge transfer related to Cu^{+} or Cu^{2+} cations stabilized by the zeolite framework.[30,31] The bands in the range of 260–550 nm proved the presence of the CuO species and $[Cu\text{-}O\text{-}Cu]^{2+}$ species.[32,33] The absorption in the range 550–900 nm is related to the d-d transitions of Cu^{2+} ions in pseudo-octahedral coordination (e.g., $Cu(H_2O)_6^{2+}$).[30,31] Clearly, for the materials with ZSM-5 synthesized at higher temperatures, the two maxima appear centered at ca. 217 and 245 nm (ascribed to the presence of Cu^{+} and/or Cu^{2+} ions, respectively). With increasing copper loading, from 2.1 wt.% for Cu-ZSM-5-com to 3.2-3.5 wt.% for Cu-ZSM-5-100(120), the bands grew in intensity and shifted to higher wavelength from Cu-ZSM-5-com to Cu-ZSM-5-100, indicating a decrease in the dispersion of copper species throughout the zeolite crystals.

To further differentiate between isolated and aggregated copper species we utilized TPR-H_2. Figure 6b depicts the TPR-H_2 profiles for our Cu-containing ZSM-5 materials. Although it is difficult to differentiate the nature of copper species located in different sites, the identification of Cu species could be attained by comparing TPR-H_2 results with the literature data. The low-temperature peaks (<300 °C) are assigned to the reduction of isolated Cu^{2+} to Cu^{+} ions and to the reduction of CuO to Cu^{0}.

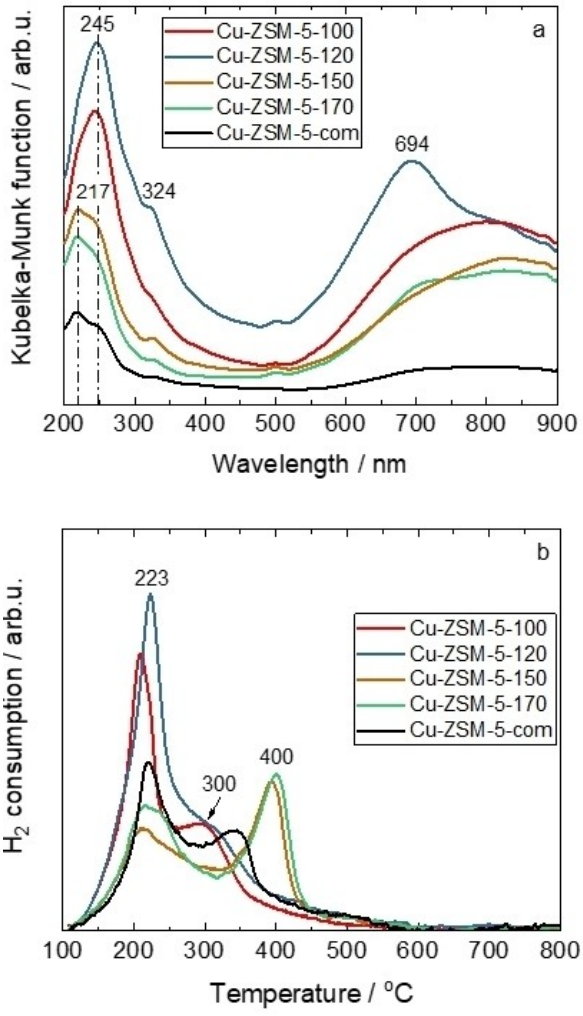

Figure 6. a) DR UV-Vis spectra and b) TPR-H_2 profiles of Cu-containing ZSM-5.

The peaks above 300 °C are associated with the reduction of highly stable Cu^{+} ions to Cu^{0}.[33,34] Besides isolated Cu^{2+} and CuO species, the DR UV-Vis analysis reveals the presence of $[Cu\text{-}O\text{-}Cu]^{2+}$ species. However, Wang et al.[34] pointed out that it is not clear if the reduction of $[Cu\text{-}O\text{-}Cu]^{2+}$ species proceeds directly to Cu^{0} or *via* Cu^{+}. Otherwise, Yang et al.[35] claimed that pretreatment at 500 °C for 4 h in Ar atmosphere before TPR-H_2 led to O_2 desorption from $[Cu\text{-}O\text{-}Cu]^{2+}$, and further to high-temperature *self-reduction* of this species and conversion of a monovalent $[Cu\text{-}\square\text{-}Cu]^{2+}$ without H_2 consumption (□ represents surface oxygen vacancy species). Such species are further reduced around 350–550 °C. In our case, Cu-ZSM-5-120 reveals the highest contribution of $[Cu\text{-}O\text{-}Cu]^{2+}$ species (according to DR UV-Vis analysis), thus, we conclude that the reduction of such species appears below 300 °C (in the main reduction peak).

Furthermore, monomeric Cu^{2+} species are characterized by means of continuous wave (CW)-EPR spectroscopy. The spectra of the fully hydrated systems (Figure 7a) are due to an electron spin S = 1/2 EPR signal typical of Cu^{2+} ions. The four-line splitting of the signal (nuclear spin I = 3/2) is particularly

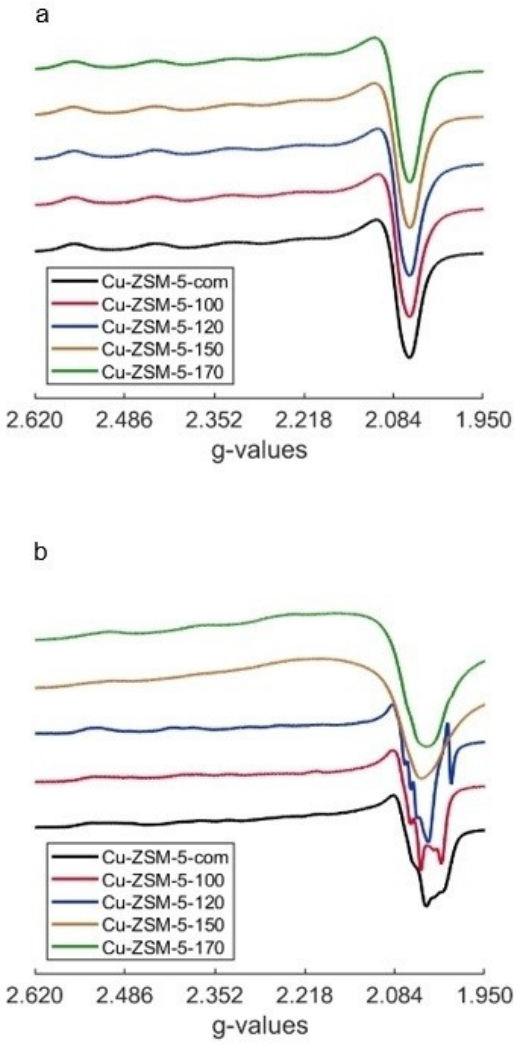

Figure 7. a) EPR spectra of hydrated Cu-containing ZSM-5 (calcined at 550 °C for 4 h in static air) recorded at −196 °C, and b) EPR spectra of fully dehydrated Cu-containing ZSM-5 (activated at 300 °C for 1 h under vacuum conditions) recorded at room temperature (ca. 25 °C).

resolved in the low-field region, in agreement with previous studies.[36,37] The experimental spectra of the hydrated samples can be reproduced by adopting an axial spin Hamiltonian model consisting of a single Cu species with parameters agreeing with the ones of hydrated Cu^{2+} ions in an octahedral geometry. It is a well-known fact that such hydrated species are able to freely move at room temperature and the motional effects are reduced by cooling down the samples.[38–40] The relative intensities of Cu^{2+} ions in the samples were determined as the double integral of the signal at −196 °C and normalized for the weight of each measured sample (Table 4). Cu-ZSM-5-170 possesses the highest concentration of isolated Cu^{2+} species followed by Cu-ZSM-5-150, Cu-ZSM-5-com, Cu-ZSM-5-100 and Cu-ZSM-5-120, respectively. These findings indicate that the samples containing the highest Al amount (Cu-ZSM-5-150 and Cu-ZSM-5-170) are also the ones capable of incorporating the highest amount of Cu^{2+} ions because of the higher probability to find two close Al sites that compensate the 2+ charge.

The spectra of the fully dehydrated samples are reported in Figure 7b. The complete removal of water molecules from the zeolite framework usually causes the narrowing of the spectral features, consistent with the decreasing mobility of copper ions. This phenomenon is particularly evident on the shape of the spectra of Cu-ZSM-5-com, Cu-ZSM-5-100 and Cu-ZSM-5-120. As well as the narrowing of the spectral linewidth, it is well-known that treatment under vacuum at T > 200 °C of Cu^{2+}-containing ZSM-5 samples causes a dropout of the intensity of the EPR signal, typically associated to the formation of EPR silent species.[39,41] Such species have been assigned to a) diamagnetic Cu^{+} ions formed by the so-called *self-reduction*,[39,42] b) $[Cu\text{-}O\text{-}Cu]^{2+}$ diamagnetic pairs ($S=0$, antiferromagnetic coupling between the two spins). The presence of these pairs or even small copper-oxygen clusters has been investigated by several authors (e.g.,[41,43]), c) $[Cu\text{-}O\text{-}Cu]^{2+}$ with $S=1$. In this case, half-field transitions have been reported around 160–170 mT.[44] It is worth noting that in all of our EPR spectra no signal at the half field due to case c) has been detected allowing us to exclude the formation of ferromagnetic Cu^{2+}-O_2-Cu^{2+}. Therefore the decrease of the EPR signal can be inferred to points a) and b). Although depletion of the EPR signal was detected for all the samples after dehydration, the spectra of Cu-ZSM-5-150 and Cu-ZSM-5-170 are more affected in comparison with the spectra of the other three samples (thus, simulation for such materials was not conducted). These findings are in agreement with *in situ* DR UV-Vis studies for Cu-ZSM-5-100 and Cu-ZSM-5-170 (see below for Figure 9), which additionally prove that the greater loss of EPR intensity is mainly attributed to the reduction of Cu^{2+} to Cu^{+} ions.

We identified three isolated Cu^{2+} complexes (*A*, *B* and *C* in Figure 8) from the spectra of dehydrated Cu-ZSM-5-com, Cu-ZSM-5-100 and Cu-ZSM-5-120 samples with spin Hamiltonian parameters very similar to the ones reported in previous studies (e.g.,[32,45]). *A* and *B* species have been assigned to isolated copper complexes in square-pyramidal configuration (likely

Table 4. H_2 consumption and EPR relative intensities of the hydrated Cu-containing ZSM-5, and turnover frequency (TOF) at NO conversion below 20%.

Samples	H_2 consumption/mmol g^{-1}	Normalized intensities	TOF (125 °C) $10^{-3}/s^{-1}$
Cu-ZSM-5-100	0.23	0.14	0.0131
Cu-ZSM-5-120	0.33	0.10	0.0136
Cu-ZSM-5-150	0.27	0.72	0.0650
Cu-ZSM-5-170	0.29	1.00	0.0593
Cu-ZSM-5-com	0.26	0.56	–

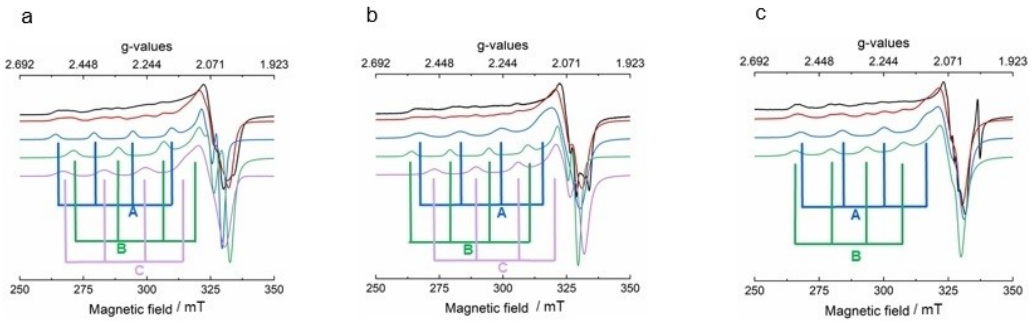

Figure 8. Experimental EPR spectra (black) and their simulation (red) of fully dehydrated a) Cu-ZSM-5-com, b) Cu-ZSM-5-100, and c) Cu-ZSM-5-120. The simulations are the result of the weighted sum of three species *A* (blue), *B* (green) and *C* (purple). The location of the four parallel hyperfine peaks is reported for each species.

Table 5. Spin Hamiltonian parameters employed for the simulations of Cu species in the dehydrated Cu-ZSM-5-com, Cu-ZSM-5-100, and Cu-ZSM-5-120.

Samples	Weight	$g\perp$	$g_{//}$	$A\perp$/MHz	$A_{//}$/MHz
Cu-ZSM-5-100	*A* 50 %	2.072 ± 0.003	2.310 ± 0.002	40 ± 10	503 ± 5
	B 10 %	2.069 ± 0.003	2.345 ± 0.002	40 ± 10	490 ± 5
	C 40 %	2.069 ± 0.003	2.260 ± 0.002	50 ± 10	510 ± 5
Cu-ZSM-5-120	*A* 50 %	2.072 ± 0.003	2.310 ± 0.002	40 ± 10	510 ± 5
	B 50 %	2.069 ± 0.003	2.354 ± 0.002	40 ± 10	450 ± 5
Cu-ZSM-5-com	*A* 50 %	2.069 ± 0.003	2.310 ± 0.002	40 ± 10	503 ± 5
	B 10 %	2.069 ± 0.003	2.345 ± 0.002	40 ± 10	490 ± 5
	C 40 %	2.070 ± 0.003	2.260 ± 0.002	50 ± 10	510 ± 5

differing in the crystal-field symmetry) located in α six-membered rings, whereas species *C* is assigned to isolated Cu^{2+} with a square-planar configuration.[45,46] The spin Hamiltonian parameters together with the weight of each single species adopted for simulating the experimental spectra are reported in Table 5. Interestingly, the spectral features of Cu-ZSM-5-120 are adequately simulated by employing only species *A* and *B*. This is consistent with the lower amount of isolated Cu^{2+} identified with respect to the other samples. Indeed species *A* and *B* are claimed to be present at lower Cu^{2+} loading whereas species assigned to *C* appear at higher copper concentration.[45]

Self-reduction of Cu^{2+} species to Cu^{+} is followed in *in situ* DR UV-Vis studies where the Cu-containing ZSM-5 were first pretreated in O_2 at 350 °C for 0.5 h. Then the O_2 was switched to N_2, and the spectra were collected in decreasing temperature. For the pretreated Cu-ZSM-5-170, the presence of copper ions in the form of exchangeable cations Cu^{2+} is documented by the bands centered at ca. 255 nm. Changing the atmosphere from oxidizing (O_2) to reducing (N_2), and the decreasing the temperature, results in a decrease in the intensity of the 255 nm band and the appearance of a new intense band at 220 nm, which we ascribe to the Cu^{+} cations (Figure 9). In contrast, for the pretreated Cu-ZSM-100 such a significant reduction of Cu^{2+} ions to Cu^{+} is not observed. In this material, copper species bears the form of oxide species: a higher value of *n*(Si)/*n*(Al) ratio than for Cu-ZSM-5-170 facilitates the hydrolysis and formation of oxospecies not prone to reduction in the nitrogen atmosphere. Nevertheless, the shift of the Cu^{2+} bands towards lower wavelengths (from 245 nm to 235 nm) indicates for the reduction of certain Cu^{2+} fractions. However, this effect is negligible when compared to the results obtained for Cu-ZSM-170, which suggests that it is the *self-reduction* process of Cu^{2+} to Cu^{+} cations.

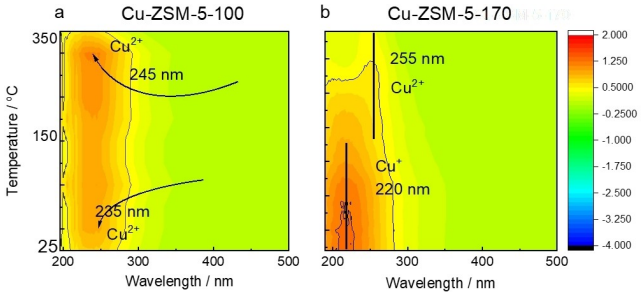

Figure 9. *In situ* DR UV-Vis spectra documenting *self-reduction* of Cu^{2+} to Cu^{+} in a) Cu-ZSM-5-100 and b) Cu-ZSM-5-170.

Catalytic studies

Figure 10 presents the results of the catalytic tests of Cu-containing ZSM-5. The catalytic activity significantly increases for the materials with ZSM-5 synthesized at high temperatures,

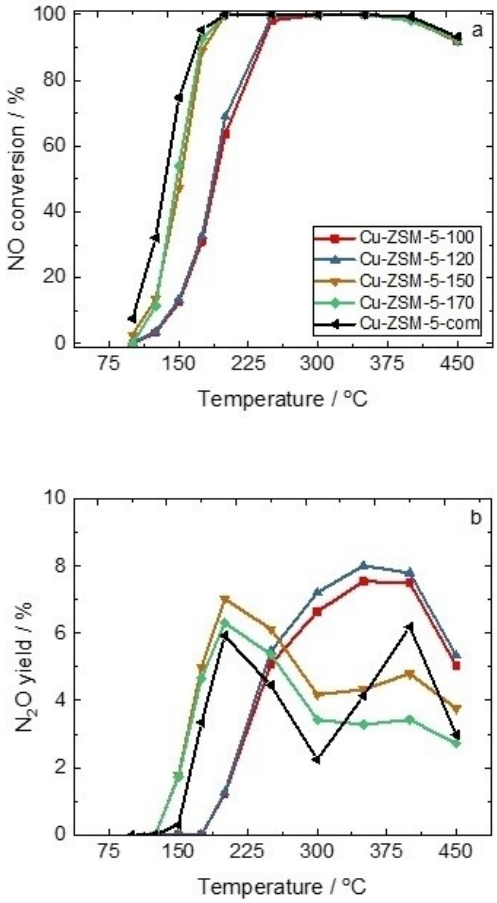

Figure 10. Results of catalytic studies: a) NO conversion and b) N_2O yield; reaction conditions: $m_K = 0.2$ g, $F_{TOT} = 120$ ml min^{-1}, c(NO) = 500 ppm, $c(NH_3) = 575$ ppm, $c(O_2) = 4$ vol.%, $c(H_2O) = 5$ vol.%, He balance, GHSV = 30 000 h^{-1}.

i.e., 150 and 170 °C as well as for the commercially-based catalyst. The obtained activity is in straight correlation with the copper content and thus related copper species content. N_2O is a major side product during NH_3-SCR-DeNO$_x$. Figure 10b displays N_2O outlet concentration as a function of temperature during the reaction. For the materials with ZSM-5 synthesized at 150–170 °C, two maxima at 175–250 °C and 350–450 °C can be identified. Otherwise for Cu-ZSM-5-100(120) broad maximum above 300 °C can be identified. The N_2O formation at lower temperatures (< 300 °C) originates mainly from the decomposition of NH_4NO_3 (e.g.,[47]), while above 300 °C comes mainly from the oxidation of NH_3. Since our Cu-ZSM-5-100(120) catalysts contain a higher content of aggregated copper oxide species compared to Cu-ZSM-5-150(170), thus, higher NH_3 oxidation over these catalysts can be expected. To compare the catalytic activity of the samples independent from the copper content, we performed the calculations of turnover frequency (TOF) at NO conversion below 20% at 125 °C (Table 4). The calculations were done with the assumption that each Cu atom (based on ICP-OES analysis) acts as an active center. The difference is significant after normalization, i.e., it can be seen that the materials based on ZSM-5, synthesized at higher temperatures, 150/170 °C, exhibit significantly higher activity than Cu-ZSM-5-100(120). The TOF for commercially based catalysts reaches $0.0469 \cdot 10^{-3}$ s^{-1} at 100 °C.

The co-operative behavior of NH_3-SCR-DeNO$_x$ co-ligands is followed precisely by 2D COS (two-dimensional correlation spectroscopy) maps obtained from the correlations of the 2300–1350 cm^{-1} spectral region typical for N═O, N–O, NH_3, NO_3, NO_2 both stretching and bending vibrations, respectively (Figure 11).

The intensity of asynchronous 2D correlation map represents the simultaneous or coincident changes of two separate spectral intensity variations measured at ν_1 and ν_2 during the specific time of the externally defined perturbation. The 2D synchronous map shows the positive autopeaks and the positive or negative cross-peaks. The positive cross-peaks represent the simultaneous changes in the intensities of the ν_1 and ν_2 bands, that is, their simultaneous increase or decrease. The negative cross-peaks represent the band intensity changes at the expense of one to the other. The intensity of an asynchronous spectrum represents sequential or successive changes of spectral intensities measured separately at ν_1 and ν_2. It provides useful information on the sequential order of events observed by the spectroscopic technique along with the external variable.

The interaction of the Cu-containing zeolites with each NH_3-SCR-DeNO$_x$ reagent is indeed documented in the FT-IR spectrum. In NO molecule the one-electron occupies the π^*-orbital causing a great NO sensitivity to the electronic state of the cation during the formation of the M···NO bond. According to the literature,[48,49] the Cu^{2+}(NO) mononitrosyl species give their FT-IR signatures in the spectral range of 1964–1845 cm^{-1}. Several types of Cu^{2+} cations have been detected by NO on Cu-containing ZSM-5. Generally, their relative concentration is dependent on the degree of exchange and the n(Si)/n(Al) ratio. The bands are at 1912–1905 cm^{-1} and originate from nitrosyls of Cu^{2+} isolated ions[42,50,51] in a square pyramidal configuration balanced by the negative charge of the two AlO_4^- tetrahedral. Similarly, the bands at 1898–1895 cm^{-1} are assigned to isolated Cu^{2+} cations, but in a square-planar configuration.[36,52] The latter cations are also supposed to coordinate O^{2-} anion (i.e., the structure of the adsorption site is $Cu^{2+}(O^-)$ or OH^- species.[42,52] In the same spectra region the bands of more complex species can be also found, e.g., $[Cu(OH)(NH_3)_{n-1}(NO)]^+$ mixed-ligand intermediate has been revealed at 1895 cm^{-1}.[12] In the most active catalyst - Cu-ZSM-5-170, the appearance of the copper(II) mononitrosyls as the primary NH_3-SCR-DeNO$_x$ reaction intermediate is documented by the correlation peaks at 1845 cm^{-1}. In less active Cu-ZSM-5-100 catalyst, three kinds of mononitrosyls participating in NH_3-SCR-DeNO$_x$ are differentiated: all of them differ in the N–O bond activation extent what is manifested by their lower frequency (1922, 1870, and 1834 cm^{-1}) concerning mononitrosyls in Cu-ZSM-5-170. These species can be formed on copper(II) ions in more clustered oxo-species or even a bidimensional CuO-like phase (1875–1868 cm^{-1}).[49]

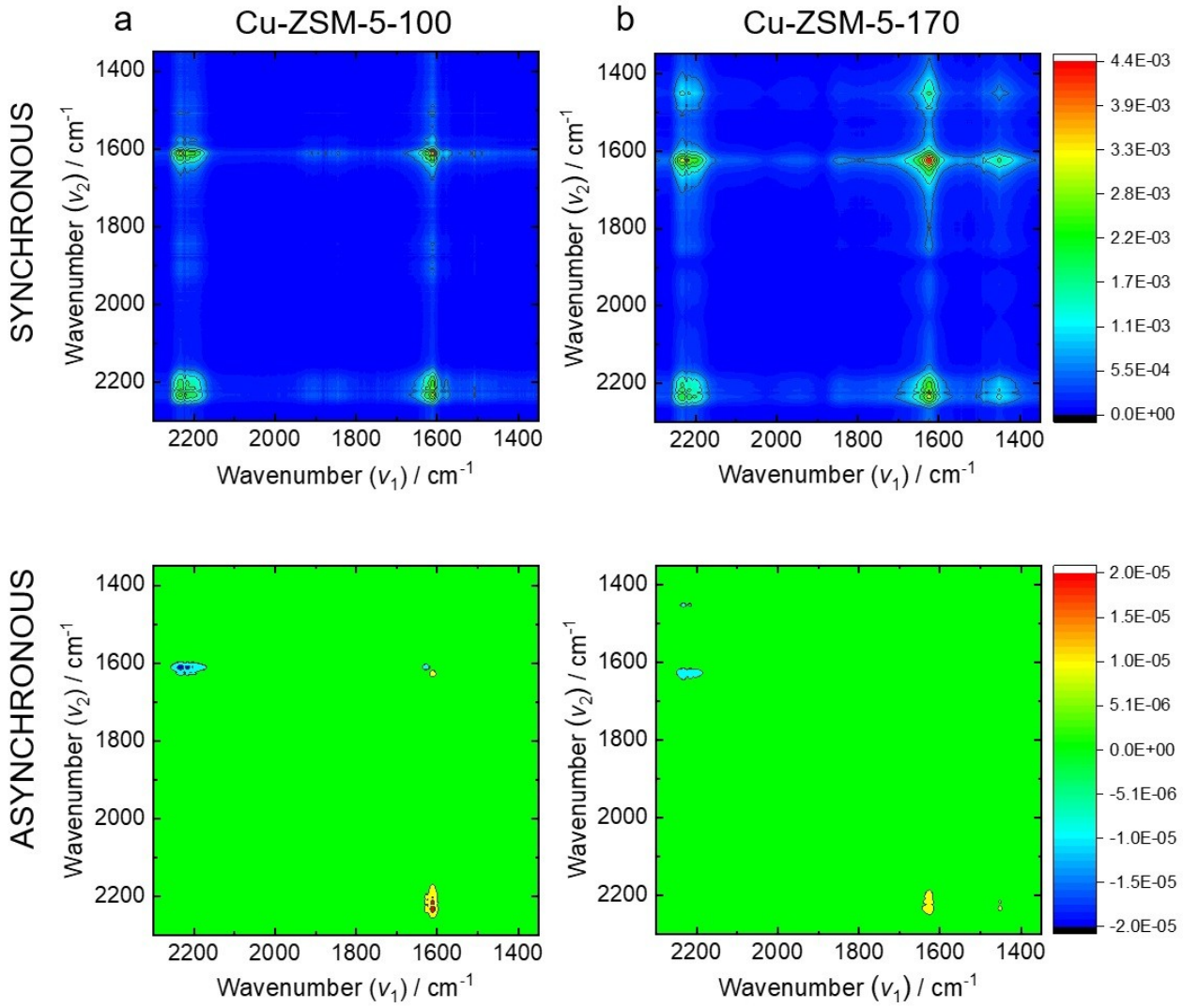

Figure 11. The 2D correlation IR spectra presenting N–O region collected upon the contact of the $c(NO):c(O_2):c(NH_3):c(H_2O) = 4:1:4:8$ mixture with a) Cu-ZSM-5-100 and b) Cu-ZSM-5-170 at 120 °C for 13 min.

The influence of co-presence of electron-donor NH_3 ligands in copper(II) coordination sphere thus the formation of $[Cu(NH_3)_3(NO)]^+$ or $[Cu(OH)(NH_3)_2(NO)]^+$ have to also be considered. Our previous studies have demonstrated that the formation of the $[Cu(OH)(NH_3)_2(NO)]^+$ mixed ligand species at 1895 cm^{-1} is governed by the competition between the O^{2-} and NH_3 ligands,[12] and also the stability of the forms initiating NH_3-SCR-DeNO$_x$, i.e., $[Cu(NH_3)_4]^{2+}$, $[Cu(OH)(NH_3)_3]^+$ and $[Cu(NH_3)_2]^+$, is determined by the interaction of ammonia molecules. In the present study, the complexity of mononitrosyls formed in Cu-ZSM-5-100 documents the heterogeneity of the forms initiating NH_3-SCR-DeNO$_x$ and also further differentiated the nature of the nitrito NO_2^- and nitrato NO_3^- moieties appearing in SCR half-cycle (1650–1350 cm^{-1}). When NO_2^-/NO_3^- is coordinated by one or two of its oxygen atoms, the corresponding species are called nitrito/nitrato monodentate and bidentate bridging or chelating compounds, respectively.

If coordination with Cu^{2+} is realized *via* its N atom, the species formed are called nitro compounds. Analysis of the available literature data shows that, in many cases, the 1635–1625 cm^{-1} band is assigned to bidentate nitrates whereas the lower frequency bands at 1575–1520 cm^{-1} can arise both from monodentate nitrates and alternatively to nitro species.[49] Typical of organic nitro compounds is a band around 1550 cm^{-1}.[53] Monodentate NO_2^- are identified by the 1448 cm^{-1} band while its bidentate counterpart is by the 1507 cm^{-1} band. Very often, the formation of NO_2^- and NO_3^- is accompanied by the generation of water because these moieties replace surface OH groups. They are also very stable and even the water co-presence does not hinder their formation. However, coadsorbed water can influence the N=O stretching modes: the respective bands are shifted toward lower frequencies in the presence of water as co-reagent.[54] Similarly, co-adsorption of strongly basic ammonia co-reactant affects the shape and the position of

these bands. The evolution of water during NH_3-SCR-DeNO$_x$ process is identified by the appearance of the band at 1635–1620 cm^{-1}, thus in the region typical of NO_3^- species. The N_2O with the respective N≡N stretching vibrations at 2224 cm^{-1}[55] is the last product species observed in 2D correlation spectra. Cu-ZSM-5-100 exhibits more heterogeneity of the forms of mononitrosyls initiating NH_3-SCR-DeNO$_x$ which is reflected also in the variety of NO_x^- species identified by the bands at 1490, 1504 and 1577 cm^{-1}, respectively. Detection of mononitrosyls and NO_2^- together with NO_3^- indicates the lower reaction rate for Cu-ZSM-5-100 in comparison with Cu-ZSM-5-170. The positive synchronous correlations of the monodentate NO_3^- band (1610 cm^{-1}) with their bidentate counterparts together with the absence of such correlation peak in asynchronous map indicates for their simultaneous formation on the surface of the Cu-ZSM-5-100 catalyst. The complex band in the 1490–1450 cm^{-1} region can also arise from NH_4^+ ions vibrations. It is generally accepted that the NH_3 molecules stored on copper sites are more reactive toward the mixture of NO and O_2 than NH_3 stored on Brønsted sites.[12,48] The latter starts to react only when copper sites are free of ammonia confirming the role of NH_4^+ as an ammonia reservoir in NH_3-SCR-DeNO$_x$. Since the simultaneous formation of the band at 1610 cm^{-1} (NO_3^-) and 1490 cm^{-1} (NO_2^-/NH_4^+) is observed in 2D COS IR maps the origin of the latter band from the NH_4^+ ions is most likely.

Monodentate NO_2^- (1490 cm^{-1}) and N_2O (2224 cm^{-1}) molecules are also produced simultaneously with NO_3^-. While the formation of N_2O occurs from nitrites (1504 and 1490 cm^{-1}) simultaneously, the negative asynchronous correlation between 2224 cm^{-1} and 1610 cm^{-1} bands is indicative for the participation also NO_3^- in N_2O production but this process is coincidental. Analysis of the asynchronous map allows also concluding that water production during NH_3-SCR-DeNO$_x$ (1625 cm^{-1} band) is coupled with mononitrosyls NO_3^- (1605 cm^{-1}) but again this process is coincidental. The higher correlation level for all the peaks observed in Cu-ZSM-5-170 points to the higher reaction rate, which further is visualized by the most intense correlation for the band of the final reaction product, i.e., water (1625 cm^{-1}). Water accumulation in Cu-ZSM-5-170 is associated with the appearance of only one type of monodentate mononitrosyls (1845 cm^{-1}) still different from the ones observed in Cu-ZSM-5-100, nitrito species (1448 cm^{-1}) (no nitrates), and N_2O (2224 cm^{-1}). For the Cu-ZSM-5-170 catalyst, the production of N_2O and NO_2^- is correlated, which is documented by the positive synchronous correlation between their bands. However, in contrast to Cu-ZSM-5-100, the asynchronous map (negative correlation at 2224 cm^{-1} × 1448 cm^{-1}) provides evidence for the conversion of NO_2^- in N_2O molecules. Similarly, water molecules' appearance is followed by N_2O production on the surface of Cu-ZSM-5-100, which is documented by the negative asynchronous correlation of these moieties diagnostic bands. All these observations are in line with the catalytic tests data. To sum up, for Cu-ZSM-5-170, homogeneous sorption centers in terms of mononitrosyl and NO_x^- species are identified *via* FT-IR spectroscopy, while their stronger electron-accepting properties manifested by a stronger interaction with NH_3 and NO (the higher strength of Lewis centers) have been documented from quantitative studies of pyridine sorption.

Conclusion

The present investigation shows that the *n*(Si)/*n*(Al) framework ratio of zeolite ZSM-5 influences the nature and distribution of copper species, and thus, their activity and selectivity of Cu-containing ZSM-5 as catalysts in NH_3-SCR-DeNO$_x$. The variation in the framework *n*(Si)/*n*(Al) ratio of 19.8—50.5 was achieved *via* changes in the zeolite preparation temperature from 100 to 170 °C. The results of catalytic studies demonstrate that the ZSM-5 materials synthesized at the higher temperature, and thus lower *n*(Si)/*n*(Al) ratio (Cu-ZSM-5-150, Cu-ZSM-5-170) exhibit more than 80% NO conversion between 175–450 °C. Other catalysts, such as Cu-ZSM-5-100 and Cu-ZSM-5-120 are significantly less active, due to the presence of aggregated copper species, as revealed from DR UV-Vis, TPR-H_2 and FT-IR analyses. NH_3-SCR-DeNO$_x$ monitored *via* 2D COS analysis of IR spectroscopy reveals mononitrosyl and NO_x^- species for Cu-ZSM-5-170, and thus, a higher reaction rate on the materials with lower *n*(Si)/*n*(Al) ratio can be assumed.

Experimental Section

Catalyst preparation

The zeolite ZSM-5 was synthesized according to the procedure given before by Palčić et al.[56] Briefly, in the first step appropriate amounts of sodium aluminate ($NaAlO_2$, Sigma–Aldrich, 50–56 wt.% Al_2O_3, 37–45 wt.% Na_2O), tetrapropylammonium hydroxide (TPAOH, Alfa Aesar, 40 wt.% water solution), and water were admixed. The mixture was agitated with a magnetic stirrer until the system became clear. Thereafter, tetraethoxysilane (TEOS, Aldrich, 99 wt.%) was added to the solution and hydrolysed at 80 °C for 24 h. The final molar oxide composition of the reaction mixture was 1.23 Na_2O:9.74TPAOH:1.0Al_2O_3:43.2SiO_2:806H_2O. The final solution was transferred to Teflon-lined autoclaves and was heated at 100, 120, 150, or 170 °C, respectively. The synthesis at 100 °C was performed for 7 days. The duration of the syntheses at 120, 150, and 170 °C was 5 days. Recovered solid phases were washed with distilled water until the pH of the supernatant was 7, dried at 80 °C, and calcined at 550 °C for 4 h in static air with a heating rate of 1 °C min^{-1}. The calcined zeolites were three times ion-exchanged with ammonium nitrate solution (0.05 M, 1 h at 80 °C, 1 g zeolite per 100 ml solution). For the sake of comparison, commercial zeolite NH_4-ZSM-5 purchased from Zeolyst (CBV5524G, *n*(Si)/*n*(Al) = 25) was used in this study. The protonic form was obtained by calcining the NH_4^+-form of zeolite at 550 °C for 4 h in static air with a heating rate of 1 °C min^{-1}.

All samples were ion-exchanged with 0.05 M aqueous solution of copper(II) acetate (Alfa Aesar, 98 wt.%) at room temperature for 24 h (1 g of zeolite per 100 ml of solution). Finally, the materials were calcined at 550 °C for 4 h in static air with a heating rate of 1 °C min^{-1}. The prepared samples are further referred to as Cu-ZSM-5-100, Cu-ZSM-5-120, Cu-ZSM-5-150, Cu-ZSM-5-170, Cu-ZSM-5-com.

Catalyst physico-chemical characterization

The X-ray powder (XRD) patterns were recorded using a HUBER G670 (Rimsting, Germany) diffractometer applying Cu-K_α radiation (wavelength: 0.154 nm). The samples were measured with a scanning range of the diffraction angle 2θ between 5 and 60° in intervals of 0.005°.

Scanning electron microscope (SEM) images of the samples were performed with a LEO Gemini 1530 SEM from Zeiss (Oberkochen, Germany) using an acceleration voltage of 10 kV. Transmission electron microscopy (TEM) measurements were carried out using a JEM-2100Plus instrument from Jeol (Tokyo, Japan) operated at an accelerating voltage of 200 kV. The images were recorded with a 4 K CMOS camera from TVIPS (Gauting, Germany). The TEM is equipped with a LaB_6 cathode and a high-resolution pole piece to achieve a point resolution in TEM mode of 0.23 nm. Chemical analysis was done using an energy dispersive X-ray (EDX) Optima-T-30 detector from EDAX/Ametek (Berwyn, US). Sample preparation was performed by grinding the sample in a mortar and pestle in ethanol, and the dispersed particles were supported on a carbon coated Ni-TEM grid.

Analysis of Al, Si, or Cu content in the samples was carried out by inductively coupled plasma optical emission spectroscopy (ICP-OES) on Perkin Elmer, Optima 8000 instrument (Rodgau, Germany). The samples (ca. 20 mg) were dissolved in a mixture of HF (2 ml, 47–51 wt.%, Sigma–Aldrich), HNO_3 (3 ml, 69 wt.%, Sigma–Aldrich), and HCl (3 ml, 35 wt.%, Sigma–Aldrich) treated with microwave radiation (1 h, 200 °C). Before measurement, HF was removed by complexing with H_3BO_3 (12 ml, 99.99 wt.%, Sigma–Aldrich) under microwave radiation (5 min, 200 °C).

Solid-state nuclear magnetic resonance (NMR) spectra were recorded on a Bruker Avance 750 spectrometer (magnetic field 17.6 T, Rheinstetten, Germany) at a frequency of 195.06 MHz for ^{27}Al and 148.69 MHz for ^{29}Si. The ^{27}Al experiments were recorded at a spinning frequency of 12 kHz and a recycle delay of 0.1 s. A 1 μs pulse was used that corresponds to about a 30° pulse angle. ^{29}Si spectra were obtained with direct excitation, a 2.5 μs 90° pulse, a spinning frequency of 7 kHz and a recycle delay of 10 s. Spectra are referenced to 1 M $Al(NO_3)_3$ solution and TMS for ^{27}Al and ^{29}Si, respectively.

Nitrogen sorption isotherms were obtained at −196 °C using a MicrotracBEL Corp., BELSORP-miniX (Haan/Duesseldorf, Germany). Before the measurement, ca. 100–200 mg of the sample was activated at 250 °C and 1 Pa. The total pore volume was taken from the point $p\ p_0^{-1} = 0.9857$. The specific surface area was calculated using the Brunauer-Emmett-Teller (BET) method and the pore width distribution was obtained using the Barret-Joyner-Halenda (BJH) method. The micropore volume and specific surface area of micropores were calculated using the Harkins and Jura model (t-plot analysis, thickness range of 0.87–1.02 nm).

Diffuse reflectance UV-Vis (DR UV-Vis) spectra of the samples were recorded at room temperature at Perkin Elmer Lambda 650S UV-Vis spectrometer (Rodgau, Germany) equipped with a 150 mm integrating sphere using spectralon® (PTFE, reflective value 99%, Rodgau, Germany) as a reference. The experiments were carried out in the wavelength range of 200–900 nm with a step width of 1 nm and a slit width of 2 nm.

In situ diffuse reflectance UV-Vis (DR UV-Vis) spectra of the selected samples (Cu-ZSM-100 and Cu-ZSM-5-170) were recorded at Shimadzu UV-2600 (Berlin, Germany) spectrometer. The self-supported pellet of the samples was placed in Praying Mantis® cell. The materials were pretreated in the flow of synthetic air (30 ml min^{-1}) at 350 °C for 0.5 h. Then the gas was changed for nitrogen and the DR UV-Vis spectra of the catalysts were recorded from 350 °C to room temperature in the intervals of every 50 °C.

The temperature-programmed reduction with hydrogen (TPR-H_2) profiles were obtained using a MicrotracBEL Corp., BelCat II (Osaka, Japan). Before measurements, the sample (50 mg) was heated from room temperature to 300 °C at a heating rate of 10 °C min^{-1} in a 20 vol.% O_2 diluted in Ar with a total flow of 6 cm^3 min^{-1}. The temperature was kept constant for 0.5 h. After that, the sample was cooled to 100 °C under a pure Ar with a total flow of 20 cm^3 min^{-1}. Then the sample was reduced with 10 vol.% H_2 diluted in Ar in the temperature range between 100 to 800 °C and a heating ramp of 10 °C min^{-1} at a total flow rate of 30 cm^3 min^{-1}. After the temperature of 800 °C was reached, it was kept constant for 0.5 h. Subsequently, the catalyst was cooled in an inert atmosphere. A thermal conductivity detector (TCD) was used to measure the H_2 consumption. For every experiment, a pulse calibration of the TCD was performed.

The electron paramagnetic resonance (EPR) spectra were recorded at −196 °C with a Bruker ESP 300E spectrometer operating at a microwave frequency of 9.5 GHz. The modulation amplitude and the microwave power were kept at 5 G and 2 mW, respectively. The spectra were simulated by using the Easyspin software (version 6.0.0-dev.26, University of Washington, Seattle, WA, US).[57] An axial spin Hamiltonian model was used for the simulation of each spectrum with a Lorentzian line shape and an equal line width for all the species. The dehydrated samples were obtained by placing about 3–20 mg of Cu-containing ZSM-5 into a 4 mm cell tube connected to a vacuum line and dehydrated under a dynamic vacuum at 300 °C for 1 h, reaching a final pressure of 10^{-3} mbar.

The acid properties of the catalysts, i.e., the nature, concentration, and strength of acid sites, were evaluated in quantitative Fourier transform infrared spectroscopy (FT-IR) studies of pyridine (Py) sorption. Before the studies, all materials were formed into self-supporting discs (ca. 5 mg^{-1} cm^2) and *in situ* thermally treated in a custom-made quartz IR cell at 550 °C under high vacuum ($p = 10^{-5}$ mbar) for 1 h. The measurements were realized by the saturation of all acid sites in the catalyst with Py (Avantor, 99 wt.%) at 130 °C. Subsequently, gaseous and physisorbed pyridine molecules were removed by 20 min evacuation at the same temperature. The concentrations of both Brønsted and Lewis acid sites were calculated from the maximum intensities of the PyH^+ (1545 cm^{-1}) and Py-L (1460-1445 cm^{-1}) bands and corresponding values of the absorption coefficients.[58] The intensity of the Si-OH groups' band was calculated by integration of their bands in the 3750–3730 cm^{-1} region in the IR spectra. All the FT-IR spectra were recorded with a Bruker Vertex 70 (Ettlingen, Germany) spectrometer equipped with an mercury-cadmium-telluride (MCT) detector. The spectral resolution was 2 cm^{-1}, and 100 scans were accumulated per spectrum.

Time-resolved measurements were also performed on the vacuum pre-treated (550 °C, 1 h, $p = 10^{-5}$ mbar) material. The material was contacted with NO, O_2, NH_3 and H_2O mixture ($c(NO):c(O_2):c(NH_3):c(H_2O) = 4:1:4:8$) at 120 °C. One spectrum was accumulated within 1 sec in a rapid scan FT-IR measurement (first 13 min of the NH_3-SCR-DeNO$_x$). The synchronous and asynchronous two-dimensional correlation spectroscopy (2D COS) maps were obtained with the use of software from OriginPro9.1.

Catalytic tests

The catalytic experiments were carried out in a fixed-bed quartz tube reactor (inner diameter: 6 mm, length: 200 mm). For catalytic experiments, a fraction of particle size in the range of 200–400 μm

was used. Before each experiment, the catalysts ($m_K = 0.2$ g) were activated at 350 °C for 1.5 h under a flow of 50 ml min^{-1} of He and then cooled down to 50 °C. After that, the simulated flue gas, with a total flow rate (F_{TOT}) of 120 ml min^{-1} composed of 500 ppm NO, 575 ppm NH_3 and 4 vol.% O_2, 5 vol.% H_2O and balance He, was switched on to pass through the catalyst bed. An excess of NH_3 ($c(NH_3)/c(NO) = 1.15$) was applied in order to ensure complete NO conversion. The gas hourly space velocity (GHSV) was determined to be ~30 000 h^{-1}. The reaction was carried out at atmospheric pressure and in the range of temperatures from 50 °C to 450 °C with an interval of 25–50 °C. At each temperature, the reaction was stabilized for 70 min before quantitative analysis of NO and N_2O concentration. The gas leaving the reactor is washed in a gas-washing bottle filled with concentrated phosphoric acid. The NO_x-converter was used to reduce NO_2 to NO, to measure the total concentration of NO_x. Analysis of the NO and N_2O was performed using a non-dispersive infrared sensor (NDIR) URAS 10E Fa. Hartmann und Braun. The conversion of NO (X(NO)) was determined according to the equation $X(NO) = ([c(NO)_{in}\text{-}c(NO)_{out}]/c(NO)_{in}) \times 100\,\%$, where: $c(NO)_{in}$ and $c(NO)_{out}$ – concentration of NO in the inlet and the outlet gas, respectively. The yield of N_2O ($Y(N_2O)$) was calculated based on the following equation: $Y(N_2O) = (2{*}c(N_2O)/[c(NO)_{in} + c(NH_3)_{in}]) \times 100\,\%$, where: $c(N_2O)$, $c(NO)_{in}$, $c(NH_3)_{in}$ - concentration of N_2O in the outlet gas, the concentration of NO and NH_3 in the inlet gas, respectively. The experimental uncertainty of the calculated conversion was found to be ±2% as indicated by repeated measurements of identical catalysts.

The turnover frequency (TOF) values for NH_3-SCR-DeNO$_x$ at NO conversion below 20% were calculated by the following equation: TOF (s^{-1}) = (c(NO)xX(NO)xF)/(m/m_W), where c(NO), X(NO) and F are concentration of NO (mol ml^{-1}), NO conversion (%), volumetric flow rate (ml s^{-1}), respectively. Also, m and m_W are the copper loading (g) on the catalyst and the molecular weight (63.54 g mol^{-1}) of copper, respectively.

Acknowledgements

M.J. acknowledges a DFG Research Grant JA 2998/2-1. P.C.B. & A.P. acknowledge the funding from the European Union's Horizon 2020 research and innovation program under the Marie Skłodowska-Curie Grant Agreement No. 813209 (PARACAT). A.P. acknowledges the funding of the Croatian Science Foundation under the project UIP-2019-04-4977. K.G.M. acknowledges Grant No. 2021/41/B/ST4/00048 from the National Science Centre, Poland. For the purpose of Open Access, the author has applied a CC-BY public copyright license to any Author Accepted Manuscript (AAM) version arising from this submission. Open Access funding enabled and organized by Projekt DEAL.

Conflict of Interest

The authors declare no conflict of interest.

Keywords: ZSM-5 · copper species · NH_3-SCR · 2D COS analysis

[1] G. Busca, L. Lietti, G. Ramis, F. Berti, *Appl. Catal. B* **1998**, *18*, 1–36.
[2] P. G. W. A. Kompio, A. Brückner, F. Hipler, G. Auer, E. Löffler, W. Grünert, *J. Catal.* **2012**, *286*, 237–247.
[3] S. M. Lee, S. S. Kim, S. C. Hong, *Chem. Eng. Sci.* **2012**, *79*, 177–185.
[4] K. Leistner, O. Mihai, K. Wijayanti, A. Kumar, K. Kamasamudram, N. W. Currier, A. Yezerets, L. Olsson, *Catal. Today.* **2015**, *258*, 49–55.
[5] J. H. Kwak, R. G. Tonkyn, D. H. Kim, J. Szanyi, C. H. F. Peden, *J. Catal.* **2010**, *275*, 187–190.
[6] F. Gao, E. D. Walter, M. Kollar, Y. Wang, J. Szanyi, C. H. F. Peden, *J. Catal.* **2014**, *319*, 1–14.
[7] F. Gao, N. M. Washton, Y. Wang, M. Kollár, J. Szanyi, C. H. F. Peden, *J. Catal.* **2015**, *331*, 25–38.
[8] J. Feng, D. Shi, Z. Xu, J. Wang, Y. Wang, X. Li, *J. Phys. Chem. A.* **2020**, *94*, 1797–1803.
[9] C. Fan, Z. Chen, L. Pang, S. Ming, X. Zhang, K. B. Albert, P. Liu, H. Chen, T. Li, *Appl. Catal. A* **2018**, *550*, 256–265.
[10] C. Torre-Abreu, M. F. Ribeiro, C. Henriques, G. Delahay, *Appl. Catal. B* **1997**, *12*, 249–262.
[11] Y. Zhu, B. Chen, R. Zhao, Q. Zhao, H. Gies, F.-S. Xiao, D. De Vos, T. Yokoi, X. Bao, U. Kolb, M. Feyen, S. Maurer, A. Moini, U. Müller, Ch. Shi, W. Zhang, *Catal. Sci. Technol.* **2016**, *6*, 6581–6592.
[12] K. A. Tarach, M. Jabłońska, K. Pyra, M. Liebau, B. Reiprich, R. Gläser, K. Góra-Marek, *Appl. Catal. B* **2021**, *284*, 119752.
[13] Y. Mao, Z. Wang, H.-F. Wang, P. Hu, *ACS Catal.* **2016**, *6*, 7882–7891.
[14] X. Wu, H. Meng, Y. Du, J. Liu, B. Hou, X. Xie, *J. Catal.* **2020**, *384*, 72–87.
[15] F. Gao, D. Mei, Y. Wang, J. Szanyi, C. H. F. Peden, *J. Am. Chem. Soc.* **2017**, *139*, 4935–4942.
[16] J. H. Kang, D. Xie, S. I. Zones, M. E. Davis, *Chem. Mater.* **2020**, *32*, 2014–2024.
[17] N. G. Vargas, S. Stevenson, D. F. Shantz, *Microporous Mesoporous Mater.* **2013**, *170*, 131–140.
[18] A. Palčić, B. M. Szyja, M. Mičetić, T. Čendak, M. Akouche, K. Juraić, M. Čargonja, D. Mekterović, V. Vušak, V. Valtchev, *Inorg. Chem. Front.* **2019**, *6*, 2279–2290.
[19] A. B. Pinar, R. Verel, J. Perez-Pariente, J. A. van Bokhoven, *Microporous Mesoporous Mater.* **2014**, *193*, 111–114.
[20] J. Kanellopoulos, A. Unger, W. Schwieger, D. Freude, *J. Catal.* **2006**, *237*, 416–425.
[21] V. Pashkova, S. Sklenak, P. Klein, M. Urbanova, J. Dědeček, *Chem. Eur. J.* **2016**, *22*, 3937–3941.
[22] P. Sarv, C. Fernandez, J.-P. Amoureux, K. Keskinen, *J. Phys. Chem.* **1996**, *100*, 19223–19226.
[23] J. Dedecek, S. Sklenak, C. Li, B. Wichterlová, V. Gábová, J. Brus, M. Sierka, J. Sauer, *J. Phys. Chem. C.* **2009**, *113*, 1447–1458.
[24] S. Sklenak, J. Dědeček, C. Li, B. Wichterlová, V. Gábová, M. Sierka, J. Sauer, *Angew. Chem. Int. Ed.* **2007**, *46*, 7286–7289; *Angew. Chem.* **2007**, *119*, 7424–7427.
[25] D. Freude, J. Kärger, *NMR techniques, Handb. Porous Solids.* **2002**, *1*, 465–504.
[26] M. Iwamoto, H. Yahiro, K. Tanda, N. Mizuno, Y. Mine, S. Kagawa, *J. Phys. Chem.* **1991**, *95*, 3727–3730.
[27] M. Iwamoto, H. Furukawa, Y. Mine, F. Uemura, S. Mikuriya, S. Kagawa, *J. Chem. Soc. Chem. Commun.* **1986**, 1272–1273.
[28] U. Deka, I. Lezcano-Gonzalez, B. M. Weckhuysen, A. M. Beale, *ACS Catal.* **2013**, *3*, 413–427.
[29] B. F. Mentzen, G. Bergeret, *J. Phys. Chem. C.* **2007**, *111*, 12512–12516.
[30] Q. Huo, D. I. Margolese, G. D. Stucky, *Chem. Mater.* **1996**, *8*, 1147–1160.
[31] L. Martins, R. P. S. Peguin, M. Wallau, E. A. Urquieta González, *Stud. Surf. Sci. Catal.* **2004**, *154*, 2475–2483.
[32] M. Jabłońska, K. Góra-Marek, M. Grilc, P. C. Bruzzese, D. Poppitz, K. Pyra, M. Liebau, A. Pöppl, B. Likozar, R. Gläser, *Catalysts.* **2021**, *11*, 843.
[33] A. Palčić, P. C. Bruzzese, K. Pyra, M. Bertmer, K. Góra-Marek, D. Poppitz, A. Pöppl, R. Gläser, M. Jabłońska, *Catalysts.* **2020**, *10*, 506.
[34] H. Wang, R. Xu, Y. Jin, R. Zhang, *Catal. Today.* **2019**, *327*, 295–307.
[35] X. Yang, X. Wang, X. Qiao, Y. Jin, B. Fan, *Materials (Basel).* **2020**, *13*, 888.
[36] J. Dedecek, Z. Sobalik, Z. Tvaruazkova, D. Kaucky, B. Wichterlova, *J. Phys. Chem.* **1995**, *99*, 16327–16337.
[37] E. Fernández, M. Moreno-González, M. Moliner, T. Blasco, M. Boronat, A. Corma, *Top. Catal.* **2018**, *61*, 810–832.
[38] P. J. Carl, S. C. Larsen, *J. Catal.* **1999**, *182*, 208–218.
[39] S. C. Larsen, A. Aylor, A. T. Bell, J. A. Reimer, *J. Phys. Chem.* **1994**, *98*, 11533–11540.
[40] E. Kweinor Tetteh, S. Rathilal, *Catalysts.* **2021**, *11*, 7.
[41] G. Turnes Palomino, P. Fisicaro, S. Bordiga, A. Zecchina, E. Giamello, C. Lamberti, *J. Phys. Chem. B.* **2000**, *104*, 4064–4073.
[42] H.-J. Jang, W. K. Hall, J. L. d'Itri, *J. Phys. Chem.* **1996**, *100*, 9416–9420.
[43] J. Sárkány, J. L. d'Itri, W. M. H. Sachtler, *Catal. Lett.* **1992**, *16*, 241–249.
[44] C.-C. Chao, J. H. Lunsford, *J. Chem. Phys.* **1972**, *57*, 2890–2898.

[45] M. H. Groothaert, K. Pierloot, A. Delabie, R. A. Schoonheydt, *Phys. Chem. Chem. Phys.* **2003**, *5*, 2135–2144.
[46] M. Occhiuzzi, G. Fierro, G. Ferraris, G. Moretti, *Chem. Mater.* **2012**, *24*, 2022–2031.
[47] D. Zhang, R. T. Yang, *Energy Fuels* **2018**, *32*, 2170–2182.
[48] S. Bordiga, C. Lamberti, F. Bonino, A. Travert, F. Thibault-Starzyk, *Chem. Soc. Rev.* **2015**, *44*, 7262–7341.
[49] K. I. Hadjiivanov, *Catal. Rev.* **2000**, *42*, 71–144.
[50] A. W. Aylor, S. C. Larsen, J. A. Reimer, A. T. Bell, *J. Catal.* **1995**, *157*, 592–602.
[51] M. Iwamoto, H. Yahiro, N. Mizuno, W. X. Zhang, Y. Mine, H. Furukawa, S. Kagawa, *J. Phys. Chem.* **1992**, *96*, 9360–9366.
[52] V. I. Parvulescu, P. Grange, B. Delmon, *J. Phys. Chem. B.* **1997**, *101*, 6933–6942.
[53] T. Tanaka, T. Okuhara, M. Misono, *Appl. Catal. B* **1994**, *4*, L1-L9.
[54] B. Djonev, B. Tsyntsarski, D. Klissurski, K. Hadjiivanov, *J. Chem. Soc. Faraday Trans.* **1997**, *93*, 4055–4063.
[55] K. Nakamoto, *Infrared spectra of inorganic and coordination compounds*, **1970**.
[56] A. Palčić, V. V. Ordomsky, Z. Qin, V. Georgieva, V. Valtchev, *Chem. Eur. J.* **2018**, *24*, 13136–13149.
[57] S. Stoll, A. Schweiger, *J. Magn. Reson.* **2006**, *178*, 42–55.
[58] K. Góra-Marek, K. Tarach, J. Tekla, Z. Olejniczak, P. Kuśtrowski, L. Liu, J. Martinez-Triguero, F. Rey, *J. Phys. Chem. C.* **2014**, *118*, 28043–28054.

Manuscript received: May 15, 2022
Revised manuscript received: June 14, 2022
Accepted manuscript online: June 16, 2022
Version of record online: July 11, 2022